Analysis of Progressive Damage in Cross-Ply and Quasi-Isotropic Panels Subjected to Quasi-Static Indentation

Kyongchan Song[1]
Analytical Mechanics Associates, Inc., Hampton, VA 23666

Frank A. Leone[2] and Cheryl A. Rose[3]
NASA Langley Research Center, Hampton, VA, 23681

The performance of a three-dimensional continuum damage mechanics (CDM) model for intralaminar damage, coupled with a cohesive zone model for delamination, is examined for damage prediction in cross-ply and quasi-isotropic laminated plates subjected to quasi-static transverse indentation. Details of the CDM model based on the deformation gradient decomposition (DGD) method and the finite element (FE) modeling strategy are presented and discussed. Critical features of the damage model and FE modeling approach are assessed by comparing analysis predictions to experimental data for cross-ply and quasi-isotropic panels in which damage is dominated by complex interactions between matrix cracks and delaminations.

I. Introduction

The use of composite materials is increasing in high-performance aerospace structures where both stiffness-to-weight and strength-to-weight considerations are important. The general susceptibility of composite materials to transverse impact damage is a particular concern to the aerospace industry because impact-induced subsurface damage is either difficult or not possible to detect visually from the exterior surface. Such damage can have a significant effect on the compressive performance of a structure. Furthermore, the impact problem of composite structures is complex as it involves complicated structural response, localized out-of-plane loading, possible strain-rate effects, and complex damage states [1-5]. Typical damage in impacted laminates may include a combination of transverse matrix cracks, delaminations, fiber failure, and permanent indentation deformation at the impact site.

In order to develop damage tolerant design criteria for composite structures, impact testing for material characterization is required. In accordance with the building block approach to the design of composite structures, information for the design process is gained by gathering an extensive database of progressively more complex structural configurations, without having to test a large number of full-scale prototype elements [6,7]. However, the results obtained from laboratory-scale tests cannot always be extrapolated to predict the response of large structures made from the same material because of potential nonlinear scaling effects. While scaling problems are present in many aspects of aircraft design, special consideration is required in the area of foreign object damage (FOD) resistance and damage tolerance, where the complex nature of the loading and failure mechanisms impedes the understanding of the governing phenomena. In the case of high-velocity impact events, such as hail ice or runway debris impacts, where the total contact duration of the impact event is of the same order of magnitude as the flexural waves traveling in the specimen, the dynamic response of the target is highly localized and laboratory-scale configurations can be employed to simulate the response of larger and more complex structures [4]. In the case of low-velocity impact events, such as tool drops, the contact duration of the event is much longer, and the global structural response characteristics of the target structure are more significant [5].

---

[1] Structural Analyst, Analytical Mechanics and Associates, NASA Langley Research Center, Mail Stop 188E, Member, AIAA.

[2] Research Aerospace Engineer, Structural Mechanics and Concepts Branch, NASA Langley Research Center, 8 West Taylor St., Mail Stop 190.

[3] Senior Research Aerospace Engineer, Structural Mechanics and Concepts Branch, NASA Langley Research Center, 8 West Taylor St., Mail Stop 190, Member, AIAA.

Accurate high-fidelity analysis approaches for predicting low-velocity impact damage offer the potential to aid in reducing the cost and time associated with developing damage tolerant composite structures. This potential has led to a recent emphasis on the development of finite element (FE) progressive damage analysis (PDA) methods. These methods focus on predicting the initiation and progression of the damage due to impact on composite structures, with particular emphasis on accurately representing the interactions between subcritical matrix cracking and delamination damage. Modeling approaches based on the use of both continuum damage mechanics (CDM) and discrete damage mechanics (DDM) models for representing the in-plane damage, coupled with cohesive surface elements for representing interlaminar damage have been proposed. Significant advances have been made in predictive capability where numerical predictions are shown to be in good agreement with experimental results in terms of global response, overall impact damage shape, and projected damage area. However, the predictive capability of the methods has been thoroughly evaluated in only a few cases [8-14] by detailed comparison, at the ply-by-ply and interface-by-interface level, of the predicted and experimentally observed damage. The lack of more detailed comparisons is due primarily to the limited amount of high-resolution, three-dimensional (3-D) experimental data available [11,15-17].

In this paper, analyses using a 3-D CDM model for intralaminar failure, coupled with the native Abaqus cohesive elements for interlaminar damage to simulate damage evolution in laminated specimens subjected to quasi-static transverse indentation are presented alongside test results. Here, analysis models with fiber-aligned meshes in the individual plies were used to ensure matrix crack development parallel to the fiber orientation [18-20].

First, static indentation tests, conducted to provide a more controlled development of damage than possible with dropped weight impact tests, will be described. Low-velocity impact is considered to be a quasi-static event and static indentation tests can provide useful information for interpreting a structure's response to low-speed impact [21, 22]. Additionally, static indentation testing provides the opportunity to interrupt tests to allow for detailed non-destructive examination to quantify damage development. Next, analysis predictions were compared with experimental data to assess critical features of the damage model and the FE modeling approach. Specifically, the predicted load displacement response was compared with the experimental data. Finally, predicted damage at each interface, in terms of overall shape and size, was compared with damage observed experimentally through X-ray computed tomography (CT) inspection.

II. Test Specimens, Test Apparatus, and Quasi-Static Indentation Tests

Four flat composite panels were considered in the present study. The test panels are comprised of Hexcel IM7/8552 unidirectional pre-impregnated carbon/epoxy tape material. The panels are 16-plies-thick with a nominal cured ply thickness of 0.0049 inch. Cross-ply laminates with stacking sequences of $[0_4/90_4]_S$ and $[0_2/90_2]_{2S}$ were investigated as well quasi-isotropic laminates with stacking sequences of $[+45_2/0_2/-45_2/90_2]_S$ and $[+45/0/-45/90]_{2S}$. To minimize computational requirements, stacking sequences with ply groupings were used to minimize the number of interfaces where delaminations might develop.

The test specimens measure 14 inches square. Each test specimen was clamped in the fixture described in Ref. [23] and shown in Figure 1. This fixture has been used in previous investigations, and was designed to minimize translations and rotations at the test section boundary. The square fixture has an outside dimension of 14 inches by 14 inches, and an unsupported central test section of 10 inches by 10 inches. The specimen was placed between the fixture base-plate and face-plate and was clamped in position with (24) 5/16-inch-diameter bolts that penetrate the test specimen through holes drilled in the specimen. Transverse loading was centrally applied to the test panels by an indenter with a 0.5-inch-diameter hemispherical tip. All static indentation tests were conducted with a servo-hydraulic testing machine under displacement control at a loading rate of 0.02 inch/minute. A direct current differential transducer was placed at the center of the test panel on the bottom surface to measure the transverse deflection. The experimental test configuration is shown in Figure 1.

A set of monotonic loading pathfinder indentation tests was first performed to characterize the global load-displacement response of the specimens for all four stacking sequences. One panel of each stacking sequence was loaded until significant back surface damage was observed. A typical load-displacement response obtained for a $[+45_2/0_2/-45_2/90_2]_S$ laminate is shown by the blue line in Fig. 2. Specimens of all layups exhibited similar global behavior, characterized by an initial elastic response, followed by load drops or change in slope of the load-displacement curve as damage developed. From these load-displacement responses, three load levels were identified for each layup as interesting with regards to the development of matrix and delamination damage:

1) Point A: First audible emission, prior to the first load drop or changing of the slope of the load-displacement curve.
2) Point B: After the first load drop or changing of the slope of the load-displacement curve.

3) Point C: Prior to the ultimate failure load.

Based on the pathfinder test results, an additional series of tests was conducted for each specimen stacking sequence in which the maximum load level for each test was chosen to coincide with Points A, B, and C. The measured load-displacement response of three $[+45/0/-45/90]_{2S}$ quasi-isotropic specimens loaded to different load levels is shown in Figure 2. Repeatability of the tests was demonstrated by overlaying the load-displacement responses of the individual tests, as shown in Figure 2, and comparing the loads at first audible emission and at subsequent load drops. After the indentation tests, a 4-inch by 6-inch section was cut from the center of each test specimen for ultrasonic inspection and X-ray CT inspection. These techniques were applied to provide details of the matrix and delamination damage at the different load levels. The voxel size of the X-ray/CT scans was 25 μm.

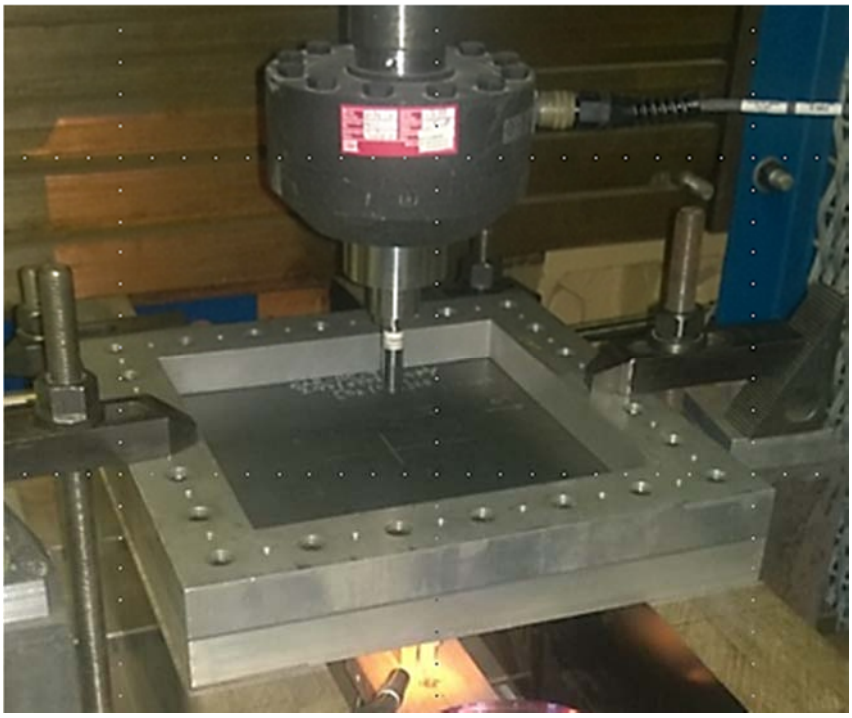

Figure 1. Static indentation test configuration.

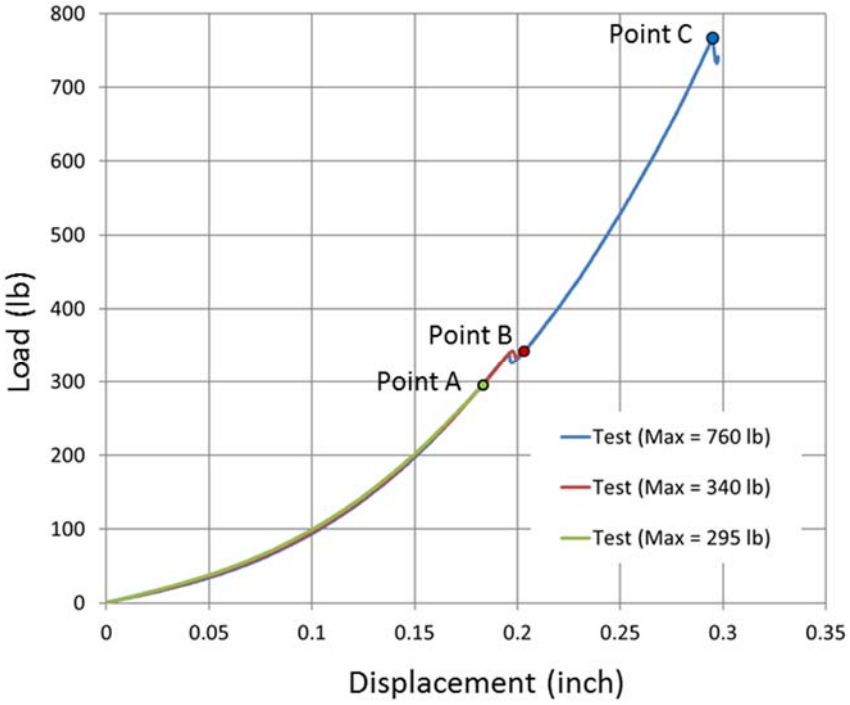

Figure 2. Load-displacement response of three quasi-isotopic panels ($[+45/0/-45/90]_{2S}$) loaded to three different maximum load levels.

III. Progressive Damage Analysis

Progressive damage analyses (PDA) were conducted using Abaqus/Explicit [24] to simulate the response of the panels subjected to transverse static indentation loading. A 3-D CDM model and standard Abaqus cohesive zone elements were used to represent intralaminar and interlaminar damage, respectively.

A. Interlaminar Damage

Delamination damage was accounted for by placing Abaqus COH3D8 cohesive elements [24] at each interlaminar interface. The constitutive response of the cohesive elements was defined by a bi-linear traction-separation law. Initially, the traction-separation law is elastic, with the traction, σ, proportional to the displacement jump, δ_{coh}, via a high penalty stiffness, K. If the displacement jump exceeds a critical value, δ_i, damage initiates and the stiffness of the cohesive element is degraded. The crack-closing forces were assumed to soften linearly such that the area under the traction-separation curve equals the fracture toughness, G_{c}. Complete separation occurs when the displacement jump exceeds, δ_f. For single-mode loading, the bi-linear cohesive law was expressed as:

$$\sigma = \begin{cases} K\delta, & \delta < \delta_i \\ (1-d^*)K\delta, & \delta_i < \delta < \delta_f \end{cases} \tag{1}$$

where the damage variable, d^*, is a function of the displacement jump and accounts for the reduction in the load-carrying ability of the material as a result of damage. The damage variable, d^*, has a value of zero when the interface is undamaged and a value of one when the interface is fully damaged.

For crack growth under mixed-mode loading, Abaqus provides options for defining damage initiation and the critical energy release rate for damage evolution. In the analyses presented herein, the onset of delamination was determined based on the quadratic stress criterion:

$$\left\{\frac{\langle\sigma_{zz}\rangle}{Y_T}\right\}^2 + \left\{\frac{\tau_{xz}}{S}\right\}^2 + \left\{\frac{\tau_{yz}}{S}\right\}^2 = 1 \tag{2}$$

where the Macaulay bracket, $< >$, indicates that a compressive normal stress, σ_{zz}, does not contribute to the damage initiation, and Y_T and S are the interlaminar normal and shear strengths, respectively. The two interlaminar shear strengths were assumed to be equal. The critical energy release rate for damage evolution was determined by the Benzeggagh-Kenane (BK) criterion [25]:

$$G_{\mathrm{c}} = G_{\mathrm{Ic}} + (G_{\mathrm{IIc}} - G_{\mathrm{Ic}})(G_{\mathrm{shear}}/G_{\mathrm{T}})^{\eta} \tag{3}$$

where η is the BK material parameter, $G_{\mathrm{shear}} = G_{\mathrm{II}} + G_{\mathrm{III}}$, $G_{\mathrm{T}} = G_{\mathrm{I}} + G_{\mathrm{II}} + G_{\mathrm{III}}$, and G_{Ic} and G_{IIc} are the fracture toughness properties for pure Mode I and Mode II fracture, respectively.

B. Intralaminar Damage

Intralaminar damage in the quasi-static indentation FE models was predicted using CompDam [26], a CDM model for fiber-reinforced materials developed at the NASA Langley Research Center in Hampton, VA. CompDam is an Abaqus/Explicit user material (VUMAT) subroutine. A key feature of CompDam is the ability to accurately represent matrix crack kinematics in geometrically nonlinear FE analyses. The kinematics of matrix cracks in CompDam are defined according to the deformation gradient decomposition (DGD) method of Leone [26,27].

Within the DGD method, the local material continuum is assumed to contain a cohesive matrix crack. The total local deformation, as described by the deformation gradient tensor, is decomposed into a reduced deformation gradient tensor for the bulk material and a cohesive displacement jump for the matrix crack. The distribution of displacement between the bulk material and matrix crack is determined by enforcing equilibrium on the matrix crack faces. After local equilibrium is satisfied, the matrix crack cohesive law is evaluated for damage progression following conventional cohesive law equations, similar to those defined in the previous section. By treating the embedded cohesive crack as a surface within the local continuum, the orientation of the matrix crack is accurately tracked even for large local shear deformations, such as when a crack is fully matured and widely open.

Matrix cracks can be inserted into the continuum with crack normals with any orientation in the local 2-3 plane. If a matrix crack orientation is not specified *a priori*, CompDam evaluates the cohesive crack initiation criterion for several possible matrix crack orientations. Once the initiation criterion is satisfied, the crack orientation is saved and the cohesive crack evolution proceeds. The cohesive crack initiation criterion in CompDam is based on the LaRC04 [28] failure criteria, taking into account the effective strengthening of the matrix material when compressive normal stresses are acting on the crack. In addition, after a cohesive matrix crack initiates, friction loads are modeled on the damaged portion of the cohesive crack.

The CompDam material model includes many additional features, including in-plane shear plasticity, fiber tensile damage, and fiber compressive fracture. However, because the quasi-static indentation problems being evaluated were dominated by interlaminar delaminations, intralaminar matrix damage, and their interactions, it was decided to only activate the CompDam features related to the insertion and evolution of intralaminar matrix damage for the presented analyses.

C. FE Models

Several FE models were developed to establish modeling requirements for properly representing the test boundary conditions, the global panel response, and for accurately predicting the development and progression of damage. In all analysis models, the fixture base-plate and face-plate were not explicitly modeled, but were represented by boundary conditions described in this section. The indenter was modeled as a rigid body associated with a reference point with mass. Contact between the between the impactor and the impacted surface of the specimen was modeled by a node to surface contact pair definition [24].

First, a baseline shell-element model, employing reduced integration S4R shell elements, was developed to identify the boundary conditions required for the analysis predictions to match the initial global stiffness of the experimental test specimens. From the baseline model, the following boundary conditions were established: the out-of-plane displacement of nodes (in the z-direction) under the supporting fixtures were fixed ($w = 0$), and nodes at the fastened bolt locations were fully clamped ($u, v, w = 0$).

A simple, combined shell- and solid-element model was then developed utilizing the shell-to-solid coupling constraints available in Abaqus. This model has two mesh regions: a global shell-element region and a local solid-element region. In the global shell-element region, which extends from the specimen boundaries to a square region centered under the indenter, reduced-integration S4R shell elements are used to represent the global displacement response of a test specimen. In the local solid-element region, reduced-integration C3D8R solid elements with enhanced hourglass control [24] were used. A mesh convergence study was conducted on a simple shell- and solid-element model to determine the size of the solid-element local region and the through-the-thickness discretization

required to properly represent the panel in-plane and bending responses. The dimensions of the solid-element local region required for a converged solution in terms of global load-displacement response were 4 inches by 4 inches, centered under the indenter. A minimum of six C3D8R elements were required through the thickness of the laminate to accurately represent the bending response of the panel. The rigid indenter, shell-to-solid coupling, and shell- and solid-element model are shown in Figure 3.

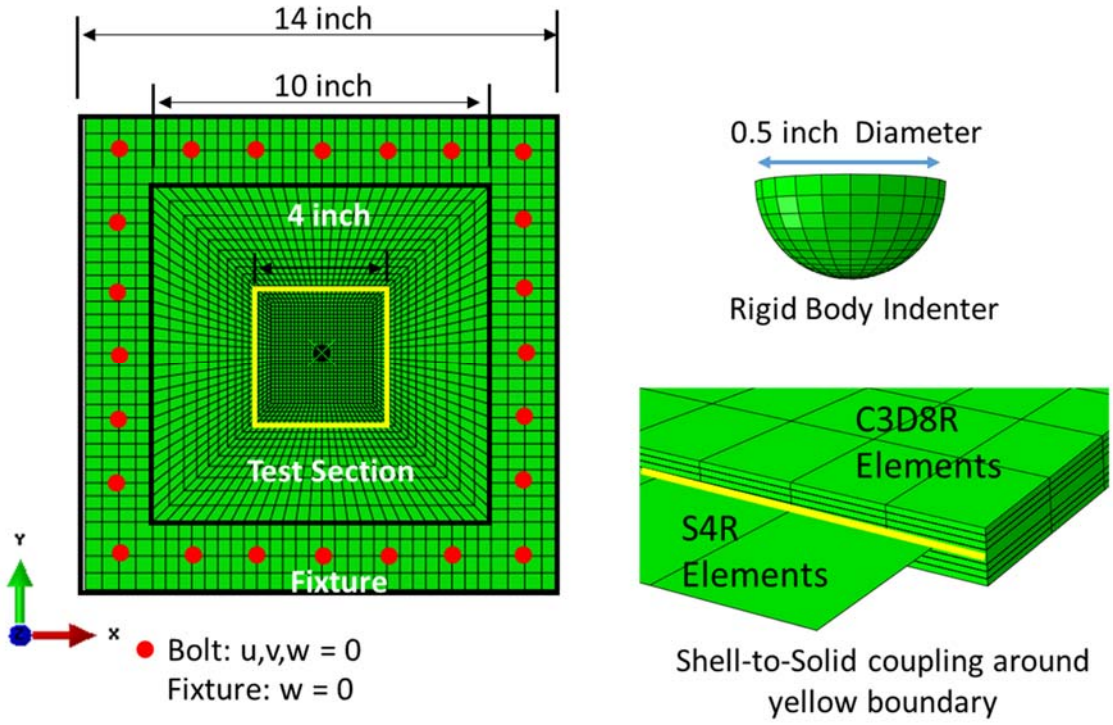

Figure 3. Rigid body indenter, shell-to-solid coupling, and simple shell-to-solid element model.

Next, a detailed combined shell- and solid-element model was developed for use in simulating coupled intralaminar and interlaminar damage progression. X-ray CT images of the panels (see for example Fig. 4) show that the damage from the static indentation loading was contained in a central area around the indenter approximately 1.3 inches square. In the detailed shell- and solid-element model, this 1.3-inch square region was meshed with C3D8R solid elements to model the individual plies, and cohesive element layers were used at the interfaces between plies. Solid elements were used to properly account for the through-the-thickness stresses, which influence the development of the impact damage. Models were built with two elements through the thickness of blocked plies of the same orientation. The through-the-thickness discretization used in the 1.3-inch-square section was also used in the 4-inch--square section. Meshes in the blocked plies were aligned with the fiber orientation to take advantage of matrix cracks propagating in the fiber direction [12, 18-20]. Tie constraints connect the individual ply meshes with the cohesive elements, and general contact was applied at each interface. Through-the-thickness discretization of the detailed shell-to-solid element model is shown schematically in Fig. 5. The solid element mesh in the 1.3-inch-square region is highly refined, having square elements with an edge length equal to 0.00787 inch. This mesh density has been recommended to accurately represent matrix crack kinematics. Intralaminar matrix damage was allowed to occur in every fourth row of solid elements, as shown in Fig. 5. This "striped" intralaminar damage approach was adopted to better represent the kinematic response of the intact material between matrix cracks. This approach also reduces the model solution times by avoiding the expense of computing intralaminar matrix damage in every solid element.

The primary emphasis of the simulations in this study was to evaluate the ability of the model to predict the interactions between matrix cracking and delamination prior to fiber failure. Therefore, fiber damage was turned off for all simulations. For computational efficiency, the displacement loading rate was between 0.23 in./sec. and 0.42 in./sec. in all analyses. A mass density of 1.5×10^{-3} lb/in^3 was used throughout the models. Also, variable mass scaling option was used with 10^{-6} desired element stable time [24]. During the simulations, the kinetic energy was

monitored to ensure that the kinetic energy did not exceed 5% of the total strain energy to ensure that significant dynamic effects were not introduced into the simulations by using relatively short total loading times.

Interlaminar fracture toughness values and material properties for IM7/8552 graphite-epoxy material were taken from Camanho [28] and are provided in Tables 1 and 2, respectively. Fracture toughness values provided in Table 1 were used for intralaminar matrix cracks as well.

Table 1. IM7/8552 Interlaminar Fracture Toughness (lbf-in/in^2) [28]

G_{Ic}	G_{IIc}
1.571	4.462

Table 2. IM7/8552 Material Properties [28]

E_{11} (Msi)	E_{22} (Msi)	G_{12} (Msi)	ν_{12}	Y_t (Msi)	Y_c (Msi)	S (Msi)
24.85	1.316	0.765	0.32	0.0090	0.02897	0.0134

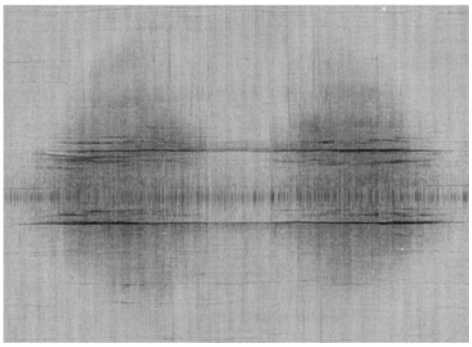

Figure 4. X-ray/CT image of the $[0_2/90_2]_{2S}$ cross-ply specimen.

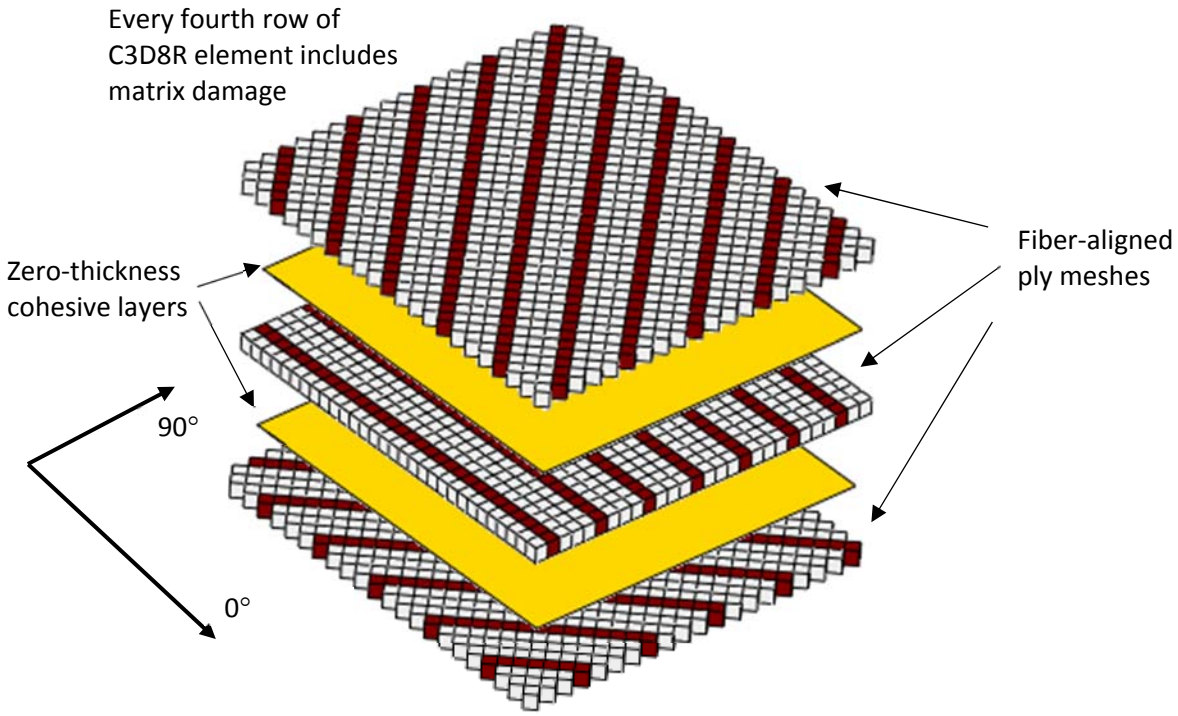

Figure 5. Through-the-thickness and in-plane discretization of the 1.3-inch square refined region.

IV. Results

Experimental and numerical results of the progressive damage analyses of the cross-ply and quasi-isotropic specimens subjected to the static transverse indentation loading are presented in this section. First, the predicted global response of the panels, in terms of the load versus displacement response, was compared with experimental data. Then, predicted intralaminar matrix and interlaminar delamination damage were compared to experimentally observed damage, characterized by X-ray/CT examination. Since the two cross-ply and the two quasi-isotropic laminates exhibited generally similar damage patterns and sequences of failure events, only the numerical and experimental results for the $[0_2/90_2]_{2S}$ cross-ply and the $[+45_2/0_2/-45_2/90_2]_S$ quasi-isotropic laminates are presented. All analyses were conducted with models having the in-plane mesh-discretization described previously, and two C3D8R solid elements through the thickness of each ply block. Discrepancies between the analysis predictions and the experimental results are described, and possible explanations for the discrepancies are provided.

A. $[0_2/90_2]_{2S}$ Cross-ply Specimen Results

The predicted load versus displacement response obtained for the $[0_2/90_2]_{2S}$ cross-ply model and experimental results from three tests are shown in Fig. 6. Test results show the first load drop occurs prior to Point B (320 lb). X-ray/CT images of the specimen loaded to 247 lb (Point A) indicate transverse matrix cracks had developed on the panel bottom surface. The X-ray/CT images of the specimen tested to 320 lb indicated that the sudden load drop at Point B corresponds to the development of matrix damage in all plies and delamination at all interfaces, except in the interface adjacent to the loaded surface. Images of the specimen tested to 555 lb (Point C) indicate additional matrix cracking and delamination growth. No fiber damage was observed. The predicted load versus displacement curve was consistent with the experimental observations, and shows the initiation of oscillations in the solution at Point A (247 lb). These oscillations were caused by dynamic forces in the explicit analysis due to the initiation and growth of matrix and delamination damage.

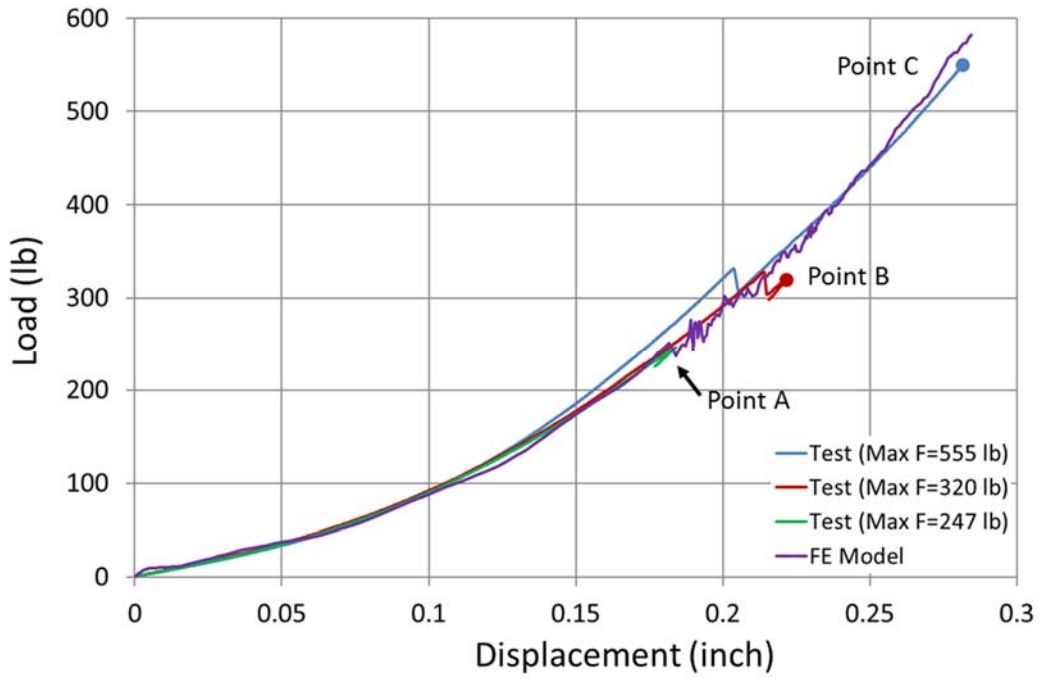

Figure 6. Experimental and predicted load versus displacement response for the $[0_2/90_2]_{2S}$ cross-ply specimen.

Damage predictions obtained with the FE model at three load levels are provided in Fig. 7. The interface beneath the loaded ply, shown in Fig. 7, is identified as interface 1, and the interface above the bottom ply is identified as interface 6. The analysis results indicate that the first major matrix crack develops at the center of the bottom surface at a low load level of 112 lb (not shown in Fig. 7). The matrix damage was then able to propagate along the fiber direction and through the thickness of the 0° layer, followed by the onset of delamination at the 90°/0° interface. With increasing load, more matrix cracks and delaminations develop in other 0° and 90° layers and at all interfaces (Point A, 247 lb). With further increase in load, additional cracks developed in the plies, and the delaminations bound by those cracks grew steadily along the fiber direction (Point B, 320 lb and Point C, 555 lb). In addition, the damage predictions of the $[0_2/90_2]_{2S}$ cross-ply model indicate that delamination tends to propagate along the fiber direction of the layer underneath the interface of interest and interacts with the matrix cracks in adjacent layers.

The predicted damage at Point B shown in Fig. 8, was compared with X-ray/CT images obtained from the test. Delaminations are shown at the indicated interface, along with matrix cracks in the adjacent plies. The analysis predictions show good qualitative agreement with the test results in terms of the projected delamination damage size, orientation, and shape. In addition, the predicted matrix crack pattern captures the dominant fiber-oriented matrix cracks observed in each ply of the experimental specimen. X-ray/CT images at each interface show symmetric damage about the indenter and no delamination damage in the area underneath the indenter at each interface. However, the analysis results show unsymmetrical delamination patterns and delamination damage in the area underneath the indenter. With increasing load, the predicted damage becomes more symmetric, similar to test observations.

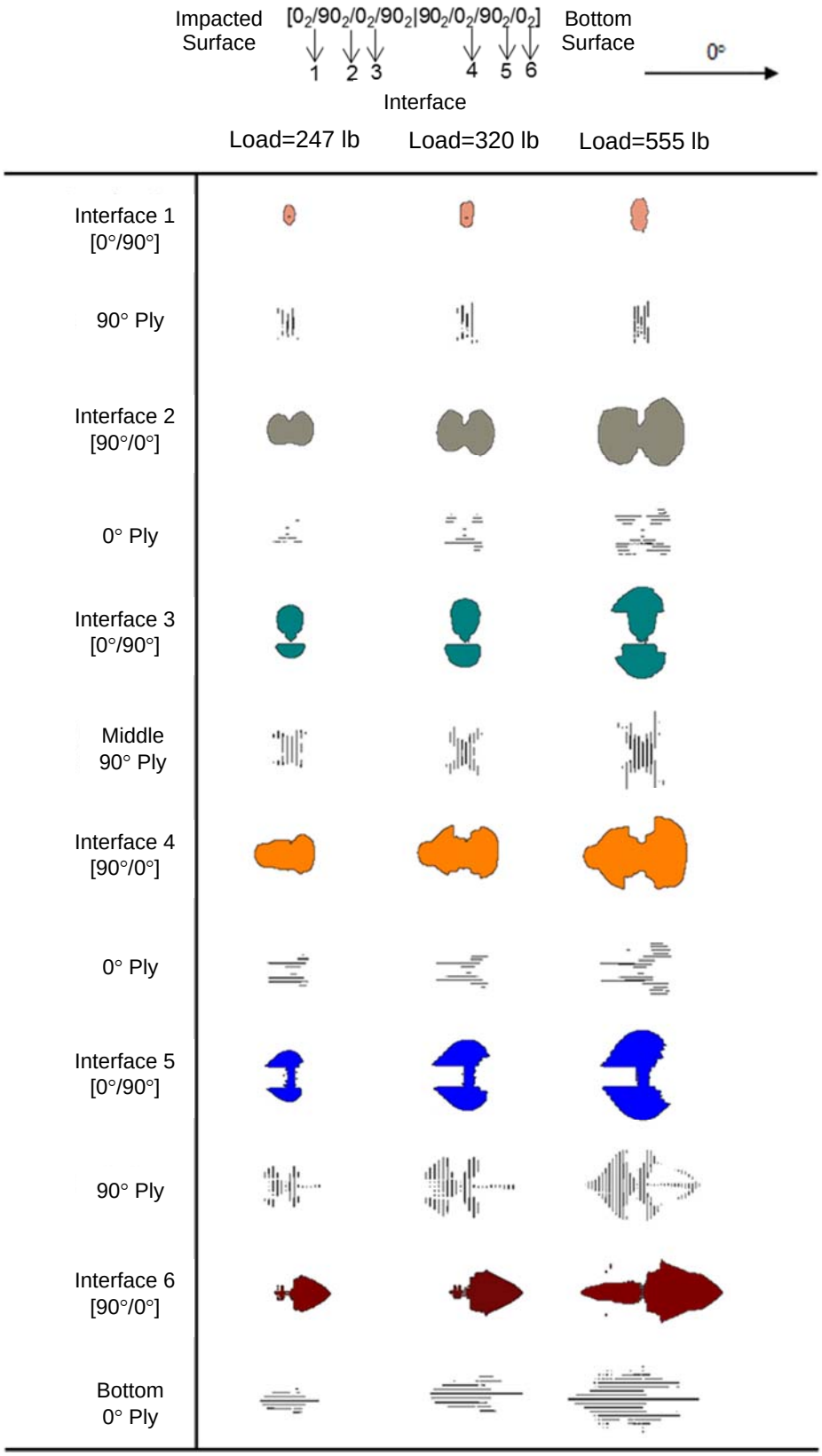

Figure 7. Interface and ply damage predictions for the $[0_2/90_2]_{2S}$ cross-ply specimen.

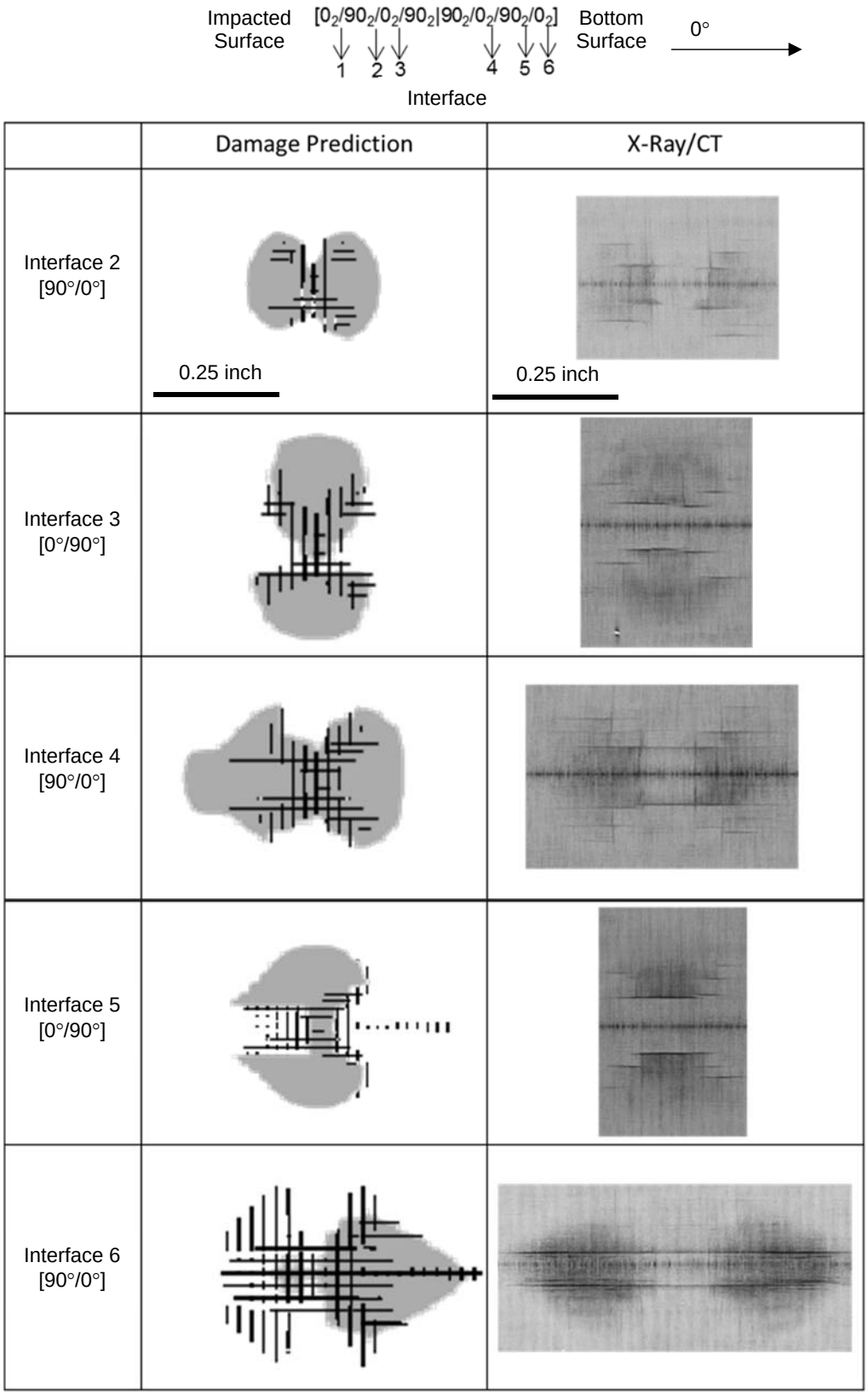

Figure 8. Experimental and predicted damage at 320 lbs (Point B in Figure 7) for the $[0_2/90_2]_{2S}$ cross-ply specimen.

B. $[+45_2/0_2/-45_2/90_2]_S$ Quasi-isotropic Specimen Results

The predicted load versus displacement response for the $[+45_2/0_2/-45_2/90_2]_S$ quasi-isotropic laminate and the corresponding experimental results from three tests are shown in Fig. 9. Audible emissions were recorded in the test at load levels just below Point A (243 lb), and a slight change in the slope of the load versus displacement curve was observed at Point B (342 lb). X-ray/CT images of the specimen loaded to Point A (243 lb) indicate a transverse matrix crack had developed at the center of the panel bottom surface, and there was a small delamination between the bottom ply and the adjacent ply. The X-ray/CT images of the specimen tested to Point B (342 lb) indicate development of matrix damage in all plies and delamination at all interfaces, except in the interface adjacent to the loaded surface. Images of the specimen tested to Point C (750 lb) indicate additional matrix cracking, delamination growth, and fiber damage in multiple plies. The predicted load versus displacement curve was consistent with the experimental observations, and shows that oscillation initiates prior to Point A (243 lb) and lasts until Point B (342 lb). The analysis results show that the matrix and delamination damage initiated in all plies and interfaces prior to Point A (243 lb). Prior to reaching Point B, all intralaminar and interlaminar damage in model links-up through the laminate thickness. The oscillations in the analysis results decrease in magnitude around Point B, after some amount of damage exists in all plies and interfaces.

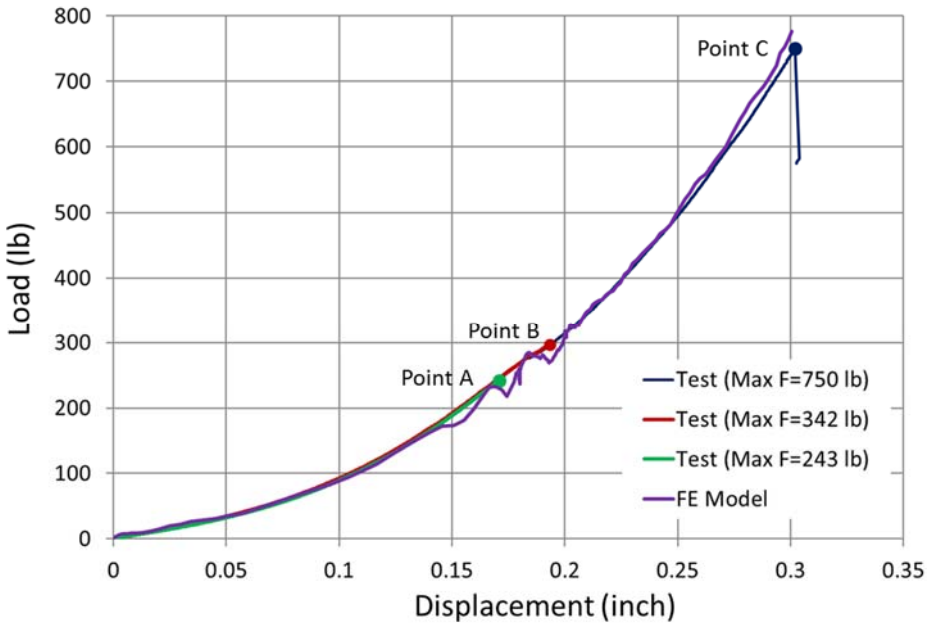

Figure 9. Experimental and predicted load versus displacement response for the $[+45_2/0_2/-45_2/90_2]_S$ quasi-isotropic specimen.

Damage predictions obtained with the FE model at three load levels are provided in Fig. 10. The interface beneath the loaded ply is identified as interface 1 in Fig. 10, and the interface above the bottom ply is identified as interface 6. The analysis results indicate that the first major matrix crack developed at the center of the bottom +45° layer at a low load level of 95 lb. The matrix damage was then able to propagate along the fiber direction, through the bottom +45°, 0°, −45°, and 90° layers thickness with additional small cracks, followed by the onset of delamination at two interfaces. Delamination onset occurs under the contacted indenter edge of top +45°/0° interface and at the bottom 0°/+45° interface, at a load level of 224 lb (not shown in Fig. 10). Delaminations formed under the indenter edge propagate outward from the edge of the indenter, and delaminations formed under the bottom 0°/+45° interface propagate along the +45° fiber direction. With increasing load, delaminations began to form in other interfaces, interacting and linking-up with the matrix cracks in adjacent layers (Point A, 243 lb). With further increases in load, link-up between delaminations and matrix cracks propagates rapidly throughout the specimen, and additional matrix cracks initiate throughout the laminate (Point B, 342 lb and Point C, 750 lb). Since the experiment was not intended for the failure of the quasi-isotropic specimen, the analysis was completed without any fiber failure within the FE model.

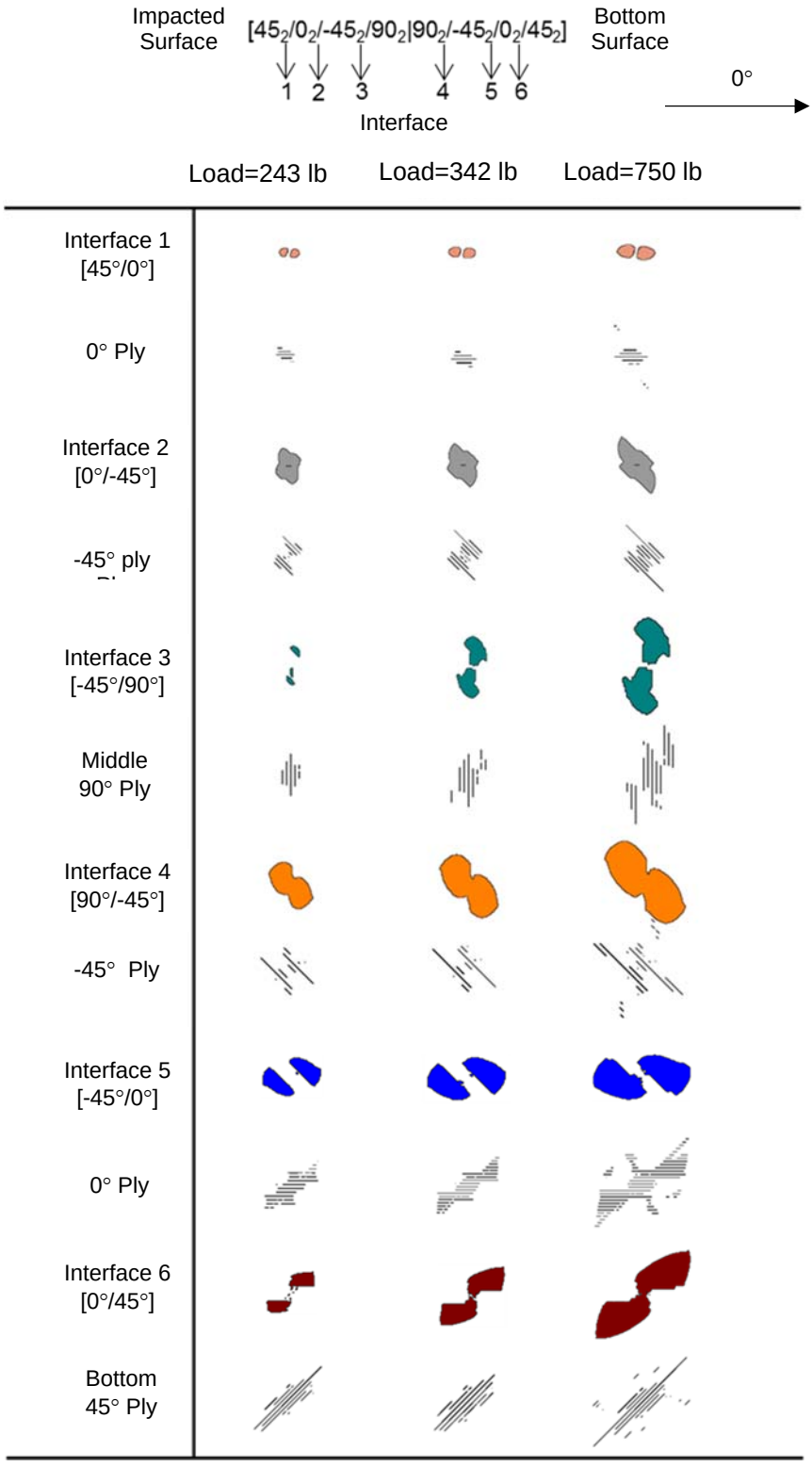

Figure 10. Interface and ply damage predictions for the $[+45_2/0_2/-45_2/90_2]_S$ quasi-isotropic model.

The predicted damage at Point B was compared with X-ray/CT images of the test specimen in Fig. 11. Delaminations were shown at the indicated interface, along with matrix cracks in the adjacent plies. In general, the analysis results tend to overestimate the delamination areas observed in the test specimens. However, the symmetric elongated delamination damage patterns along the fiber orientation of the ply below the interface were consistent with test observations. The experimental results show little delamination at interface 1, and no delaminations in the area underneath the indenter throughout the laminate. However, the numerical results show noticeable delamination similar to the predicted damage of the cross-ply model. These predicted delaminations underneath the indenter could be caused by inaccuracies in the load distribution between the analytical indenter and the top surface of the model. During the test, the indentation on the loaded surface caused a residual indentation, due to matrix plasticity and/or damage. Neither in-plane nor transverse plasticity were utilized in the FE models, resulting in the residual indentation not being captured. The lack of softening in the models due to transverse plasticity may have caused the contact area between the analytical indenter and the top surface of model to be smaller than in the test. The more-concentrated load introduction in the model could have contributed to the erroneous prediction of delamination in the area underneath the indenter. Overall, the analysis model qualitatively captures the structural response, the damage initiation, and the observed experimental damage evolution.

V. Concluding Remarks

A study on the performance of a 3-D state-of-the-art CDM model was presented in this paper. The performance study was coupled with the native Abaqus cohesive elements to simulate damage evolution in cross-ply and quasi-isotropic laminated specimens subjected to quasi-static transverse indentation. An FE model with fiber-aligned meshes in the individual plies was employed to facilitate the development of intralaminar matrix cracks parallel to the fiber orientation in the ply. The predicted global structural response as indicated by the load-displacement curve and the predicted damage evolution were compared with experimental data to assess the CDM material model and the methods for performing progressive damage FE analyses. The structural responses of the models agree well with test observations. Qualitative comparisons of the simulated damage states with X-ray/CT results indicate that the analytical models properly simulated intralaminar and interlaminar matrix damage within a laminated specimen subjected to static transverse indentation loading, in terms of the sequence of damage evolution, the pattern of intralaminar damage, and the shape of delaminations. Discrepancies between the analysis predictions and the experimental results were also noted. Improved correlation between the test and analysis results may be achieved by developing additional features for the material damage model. The ability to predict the permanent indentation underneath the indenter requires improved transverse plasticity modeling. In addition, accounting for the delayed initiation of delamination when an interface was subjected to compressive loads could improve quality of the predictions in the vicinity of the indenter.

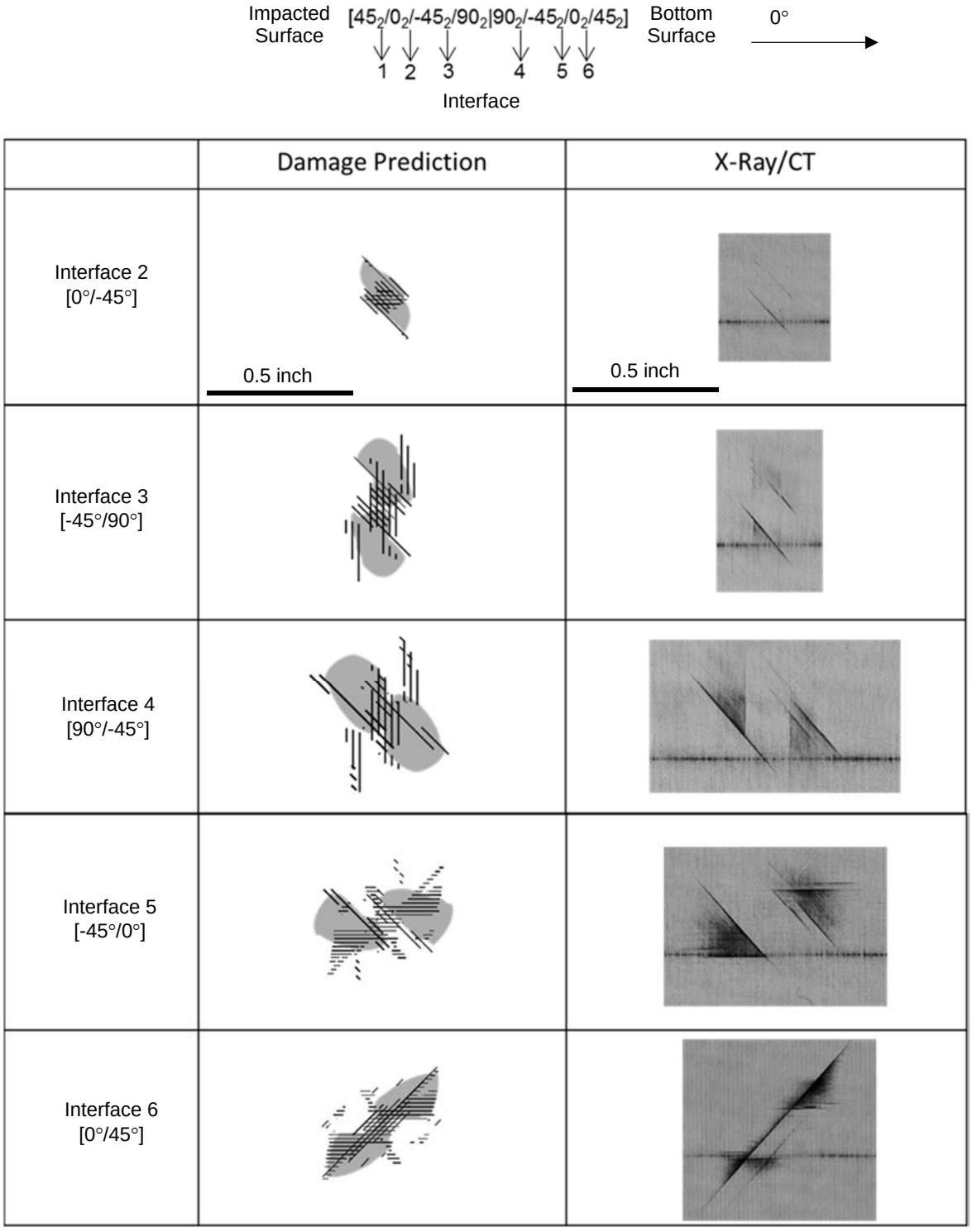

Figure 11. Experimental and predicted damage at Point B (342 lb) for the $[+45_2/0_2/-45_2/90_2]_S$ quasi-isotropic specimen.

References

[1]Abrate, S., "Impact on Laminated Composite Materials," *Applied Mech. Rev*., Vol. 44, No. 4, April 1991, pp. 155-189.

[2]Cantwell, W. J., and Morton, J., "The Impact Resistance of Composite Materials – A Review," *Composites*, Vol. 22, No. 5, September 1991, pp. 347-362.

[3]Abrate, S., *Impact on Composite Structures*, Cambridge University Press, 1998.

[4]Cantwell, W. J., "The Influence of Target Geometry on the High Velocity Impact Response of CFRP," *Composite Structures*, Vol. 10, 1988, pp. 247-265.

[5]Cantwell, W. J., and Morton, J., "Geometrical Effects in the Low Velocity Impact Response of CFRP," *Composite Structures*, 1989, pp. 39-59.

[6]Whitehead, R. S., Dee, R. B., "A Building Block Approach to Design Verification Testing of Primary Composite Structures," Proceedings of the 24th AIAA/ASME/AHS SDM Conference, Lake Tahoe, NV, May 1983, pp. 473-477.

[7] Rouchon, J., "Certification of Large Aircraft Composite Structures, Recent Progress and New Trends in Compliance Philosophy," presented at the 17th ICAS, Stockholm, Sweden, 1990.

[8]Li, C. F, Hu, N., Cheng, J. G, Fukunaga, H., Sekine, H., "Low Velocity Impact Induced Damage of Continuous Fiber-Reinforced Composite Laminates. Part II. Verification and Numerical Investigation," *Composites: Part A*, Vol. 33, 2002, pp. 1063-1072.

[9]Bouvet, C., Castanié, Bizeul, M., Barrau, J. J., "Low Velocity Impact Modelling in Laminate Composite Panels with Discrete Interface Elements," *International Journal of Solids and Structures*, Vol. 46, 2009, pp. 2809-2821.

[10]Shi, Y., Swait, T., Soutis, C., "Modeling Damage Evolution in Composite Laminates Subjected to Low Velocity Impact," *Composite Structures*, Vol. 94, 2012, pp. 2902-2913.

[11]Feng, D., Aymerich, F., "Finite Element Modelling of Damage Induced by Low-Velocity Impact on Composite Laminates," *Composite Structures*, Vol. 108, 2014, pp. 161-171.

[12]Lopes, C. S., Sádaba, S., González, C., LLorca, J., Camanho, P. P., F., "Physically-sound Simulation of Low-velocity Impact on Fiber Reinforced Laminates," *International Journal of Impact Engineering*, Vol. 92, 2016, pp. 3-17.

[13]Sitnikova, E., Li, S., Li, D., Yi, X., "Subtle Features of Delamination in Cross-Ply Laminates Due to Low Speed Impact," *Composites Science and Technology*, Vol. 149, 2017, pp. 149-158.

[14]Sun, X. C., Wisnom, M. R., Hallett, S. R., "Interaction of Inter- and Intralaminar Damage in Scaled Quasi-Static Indentation Tests: Part 2 – Numerical Simulation," *Composite Structures*, Vol. 149, 2017, pp. 149-158.

[15]Sun, X. C., Hallett, S. R., "Barely Visible Impact Damage in Scaled Composite Laminates: Experiments and Numerical Simulations," *International Journal of Impact Engineering*, Vol. 109, 2017, pp. 178-195.

[16]Wagih, A., Maimí, P., Blanco, N., Costa, J., "A Quasi-Static Indentation Test to Elucidate the Sequence of Damage Events in Low Velocity Impacts on Composite Laminates," *Composites: Part A*, Vol. 82, 2016, pp. 180-189.

[17]Abisset, E., Daghia, F., Sun, X. C., Wisnom, M. R., Hallett, S. R., "Interaction of Inter- and Intralaminar Damage in Scaled Quasi-Static Indentation Tests: Part 1 – Experiments," *Composite Structures*, Vol. 136, 2016, pp. 712-726.

[18]Jirásek, M., and Grassl, P., "Evaluation of Directional Mesh Bias in Concrete Fracture Simulations Using Continuum Damage Models," *Engineering Fracture Mechanics*, Vol. 75, No. 8, 2008, pp. 1921-1943.

[19]Las, V., and Zemcik, R., "Progressive Damage of Unidirectional Composite Panels," *Journal of Composite Materials*, Vol. 42, 2008, pp. 25-44.

[20] Song, K., Yingyong, L., and Rose, C. A., "Continuum Damage Mechanics Models for the Analysis of Progressive Failure in Open-Hole Tension Laminates," AIAA Paper No. 2011-1861, April 2011.

[21]Feraboli, P., Kedward, K. T., "Enhanced Evaluation of the Low-Velocity Impact Response of Composite Plates", *AIAA Journal*, Vol. 42/10, October 2004, pp. 2143-2152.

[22]Kwon, Y. S., and Sankar, B. V., "Indentation-Flexure and Low-Velocity Impact Damage in Graphite Epoxy Laminates," *Journal of Composites Technology and Research*, Vol. 15, No. 2, 1993, pp. 101-111.

[23]Ambur, D. R, Starnes, J. H. Jr., Prasad C. B., "Influence of Target and Impactor Parameters on the Nonlinear Response and Residual Strength of Curved Thin Composite Plates," 41st AIAA Structures, Structural Dynamics and Materials Conference, No. 2000-1591, April 2000.

[24]*Abaqus®/Standard User's Manuals*, Version 6.14, Dassault Systèmes Simulia Corp., Providence, Rhode Island, 2015.

[25] Benzeggagh, M.L. and Kenane, M., "Measurement of mixed-mode Delamination Fracture Toughness of Unidirectional Glass/Epoxy Composites with Mixed-mode Bending Apparatus," *Compos. Sci. Technology*, Vol. 56, No. 4, 1996, pp. 439–449.

[26] CompDam_DGD, version 1.0.1, https://github.com/nasa/CompDam_DGD.

[27] Leone, F., A., "Deformation Gradient Tensor Decomposition for Representing Cracks in Fiber-Reinforced Materials," *Composites Part A*, Vol. 76, 2015, pp. 334–341.

[28] Camanho, P. P., Maimí, P., and Dávila, C. G., "Prediction of Size Effects in Notched Laminates Using Continuum Damage Mechanics," Composites Science and Technology, Vol. 67, No. 13, 2007, pp. 2715-2727.